JOURNAL OF COMPUTATIONAL PHYSICS 40, 120–142 (1981)

Computation of Steady and Oscillatory Convection in Saturated Porous Media*

JOHN GARY

Computer Science Department, University of Colorado, Boulder, Colorado 80309

AND

D. R. KASSOY

Mechanical Engineering Department, University of Colorado, Boulder, Colorado 80309

Received December 3, 1979; revised July 31, 1980

We report on computational methods and results for convection of a constant property liquid in a saturated porous medium. Flow is examined in a square domain with insulated side walls, a cold top and a hot bottom boundary. An ADI finite difference method which is fourth order in space and second order in time is compared with a method of lines code which is based on fourth order finite differences in space and a Runge–Kutta–Fehlberg fourth order ODE solver. A coordinate transformation is used with the ADI scheme in an attempt to improve resolution in the boundary layer. The accuracy of the ADI method is studied by application to steady flow at Rayleigh number $R = 200$. A comparison of the methods is also made for solutions at $R = 400$, some of which display oscillations in time. An attempt is made to study the structure of these oscillatory solutions. A nearly steady "single-cell" solution at $R = 400$ is also described. We find five distinct long-time solutions at $R = 400$, each of which is generated by a different initial condition.

1. INTRODUCTION

We are concerned with the numerical solution of the equations which govern convection in a saturated porous medium which is heated from below. The steady conduction solution gives way to a steady convective flow above the critical Rayleigh number which is

$$R_c = 4\Pi^2. \tag{1}$$

This steady solution in turn gives way to an oscillatory solution, for higher Rayleigh numbers, somewhere in the range $300 \leqslant R \leqslant 400$. The nature of this convection has been studied by numerous people including Caltagirone [1], Horne [19], Horne and O'Sullivan [8, 9], Straus and Schubert [14], and Schubert and Straus [12]. Surveys

* This research was supported by NSF Grant ENG77-26893.

0021-9991/81/030120-23$02.00/0

of steady and oscillatory convection in porous media have been given recently by Combarnous and Bories [3], Combarnous [20], and Cheng [2].

Horne [19] and Horne and O'Sullivan [8, 9] have noted that long-time solutions are initial condition dependent. In a constant viscosity calculation at $R = 500$, a three-cell steady flow in a square evolved, following an impulsive rise of the uniform lower boundary temperature. In contrast when the bottom temperature was raised slowly a one-cell oscillatory solution developed. Similar results were found for other values of Rayleigh number when $R \gtrsim 280$. Flows induced in squares and rectangles with partially heated bottom boundaries are qualitatively similar. Horne and O'Sullivan [21] produced related solutions for a variable viscosity liquid as well.

Caltagirone [1] found steady solutions in rectangular domains of various aspect ratio at several specific Rayleigh numbers up to 300. Oscillatory solutions were observed near $R = 500$. A Galerkin method was used to show that the fluctuation critical Rayleigh number was about 384 for a square.

A numerical Galerkin procedure was employed by Schubert and Straus [12] to investigate a variety of two- and three-dimensional flows. They found a fluctuation critical Rayleigh number in the range $300 \lesssim R \lesssim 320$ for the strictly two-dimensional case of a single roll. Such flows are physically plausible in three-dimensional systems if the dimension perpendicular to the plane of the roll is sufficiently small. Multiple-cell steady solutions are unstable at larger values of the Rayleigh number. A unicellular oscillatory solution, with nearly harmonic variations in time, was produced at $R = 350$. At larger Rayleigh number values the time-history is less regular but definitely oscillatory. Multiplicity of solution at large Rayleigh number was observed.

In the present work we have two major goals in mind. The first is to delineate the level of accuracy of the numerical solutions developed in the past, particularly with regard to the oscillatory case. In order to achieve this goal we present a systematic comparison of second and fourth order finite difference methods and an assessment of spatial resolution. Our second goal is to ascertain the degree of multiplicity of long-time solutions at a moderate Rayleigh number larger than the fluctuation critical value.

We consider the paradigm problem of a constant viscosity liquid in a square porous medium, with insulated side walls and horizontal boundaries at constant but different temperatures.

We applied two numerical methods to the porous convection equations. To our knowledge these methods have not been used before in this setting. Both methods use a finite difference approximation in the rectangular (x, z) domain which can be either second or fourth order accurate depending on the use of either three or five mesh points to approximate spatial derivatives. The first method is an alternating-direction-implicit (ADI) method [10, 11] which is second order accurate in time and is run with a fixed time step. The second method is a Runge–Kutta–Fehlberg (RKF) (3–4) method [7, 13] which provides fourth order accuracy in time and automatically adjusts the time step in accordance with a preassigned error tolerance. To compute steady state solutions the ADI scheme was superior since a large time step could be

used to accelerate convergence. For oscillatory solutions at a Rayleigh number above 400 the RKF method is probably superior.

We have found single-cell oscillatory solutions at $R = 400$ of both harmonic and irregular form depending upon the initial conditions used to start the calculation. A single-cell steady solution was produced at $R = 400$ by slowly increasing the Rayleigh number of the system with time. Finally multiple cell steady solutions were also produced at $R = 400$.

In the case of steady state solutions a high degree of spatial resolution, obtained by using up to 50×50 mesh spacing, was employed to demonstrate code convergence. An equal degree of resolution was economically unfeasible for us in the case of the oscillatory solution at $R = 400$, given the computer available. The solutions for 20×20 and 30×30 meshes are fairly close. We really need a solution on a 40×40 mesh for a definitive result.

2. The Differential Equations

The porous flow model consists of a marching equation for the temperature deviation $\theta(x, z)$ and an elliptic equation for the stream function $\psi(x, z)$. Here θ is the deviation from the steady conduction temperature. The equations are those given by Zebib and Kassoy [15]. The variables are all non-dimensional. In our experiments the domain (x, z) is always square with $0 \leqslant x \leqslant 1$, $-1 \leqslant z \leqslant 0$. The relation between θ and the non-dimensional temperature T is $T = -z + \theta$, where $0 \leqslant T \leqslant 1$. Note that the non-dimensional time is larger by a factor of R than that commonly used. The equations are

$$\frac{\partial^2 \psi}{\partial x^2} + \frac{\partial^2 \psi}{\partial z^2} = -\frac{\partial \theta}{\partial x}, \tag{2.1}$$

$$\frac{\partial \theta}{\partial t} = \frac{1}{R}\left(\frac{\partial^2 \theta}{\partial x^2} + \frac{\partial^2 \theta}{\partial z^2}\right) - \frac{\partial \psi}{\partial x} - \frac{\partial \theta}{\partial x}\frac{\partial \psi}{\partial z} + \frac{\partial \theta}{\partial z}\frac{\partial \psi}{\partial x}. \tag{2.2}$$

Here R denotes the Rayleigh number. The boundary conditions are

$$\begin{aligned} &\theta = 0, \quad \psi = 0 && \text{at top and bottom } z = 0 \text{ and } z = -1 \\ &\frac{\partial \theta}{\partial x} = 0, \quad \psi = 0 && \text{on the sides } x = 0 \text{ and } x = 1 \end{aligned} \tag{2.3}$$

Various initial conditions for $\theta(x, z, 0)$ will be used.

The Nusselt number is a ratio of the total heat transport through a horizontal section to that due to conduction alone. It is given by the following formula

$$\mathrm{Nu}(z, t) = 1 - \int_o^1 (\theta_z(x, z, t) + R\theta(x, z, t)\, \psi_x(x, z, t))\, dx. \tag{2.4}$$

For a steady state solution the Nusselt number is independent of both z and t. Numerical errors will cause the computed Nusselt number to vary with z. It is less accurate to compute $\mathrm{Nu}(z, t)$ at the boundary ($z = -1$ or $z = 0$) because θ_z must be approximated by a one-sided difference. This difference approximation is not required to solve (2.2) since this equation is not approximated at the boundary, but only in the interior. Our results will give the Nusselt number at the boundary $\mathrm{Nu}(-1, t)$ and also the integral average

$$\bar{\mathrm{Nu}}(t) = \int_{-1}^{0} \mathrm{Nu}(z, t)\, dz. \tag{2.5}$$

The solution of the porous flow equations tends to develop a boundary layer along the edge of the domain. This suggests the use of a finer mesh near the edges. Alternatively, we can use a coordinate transformation with a constant mesh spacing. We chose the latter approach. The original mesh is denoted by (x, z), where $0 \leqslant x \leqslant 1$ and $-1 \leqslant z \leqslant 0$. The transformed coordinates are $(\hat{x}, \hat{z})$, where $-1 \leqslant \hat{x} \leqslant 1$ and $-1 \leqslant \hat{z} \leqslant 1$. The transformation is given by

$$\hat{x} = f(x), \qquad x = f^{-1}(\hat{x}), \qquad \hat{z} = g(z), \qquad z = g^{-1}(\hat{z}). \tag{2.6}$$

Then the derivatives transform according to the formula

$$\begin{aligned} \frac{\partial}{\partial x} &= F_1(\hat{x}) \frac{\partial}{\partial \hat{x}}, \qquad \frac{\partial^2}{\partial x^2} = (F_1(\hat{x}))^2 \frac{\partial^2}{\partial \hat{x}^2} + F_2(\hat{x}) \frac{\partial}{\partial \hat{x}}, \\ \frac{\partial}{\partial z} &= G_1(\hat{z}) \frac{\partial}{\partial z}, \qquad \frac{\partial^2}{\partial z^2} = (G_1(\hat{z}))^2 \frac{\partial}{\partial \hat{z}^2} + G_2(\hat{z}) \frac{\partial}{\partial \hat{z}}, \end{aligned} \tag{2.7}$$

where

$$\begin{aligned} F_1(\hat{x}) &= f'(f^{-1}(\hat{x})), \qquad F_2(\hat{x}) = f''(f^{-1}(\hat{x})), \\ G_1(\hat{z}) &= g'(g^{-1}(\hat{z})), \qquad G_2(\hat{z}) = g''(g^{-1}(\hat{z})). \end{aligned}$$

The transformed equations are (using subscripts to denote partial derivatives).

$$\theta_t = \frac{1}{R}(F_1^2 \theta_{\hat{x}\hat{x}} + G_2 \theta_{\hat{z}}) - F_1 \psi_{\hat{x}} - F_1 G_1(\theta_{\hat{x}} \psi_{\hat{z}} - \theta_{\hat{z}} \psi_{\hat{x}}) \tag{2.8}$$

$$F_1^2 \psi_{\hat{x}\hat{x}} + F_2 \psi_{\hat{x}} + G_1^2 \psi_{\hat{z}\hat{z}} + G_2 \psi_{\hat{z}} = F_1 \theta_{\hat{x}}. \tag{2.9}$$

For the calculations described in this paper we used the following coordinate transformation which is determined by the single parameter α.

$$f(x) = S \frac{(1 + \alpha S^2)}{1 + \alpha}, \qquad \text{where} \quad S = 2x - 1,$$

$$g(x) = T \frac{(1 + \alpha T^2)}{1 + \alpha}, \qquad \text{where} \quad T = 1 + 2z.$$

If $\alpha = 0$, then the transform is linear and the mesh spacing in the (x, z) coordinates is uniform. The ratio of the (x, z) mesh spacing at the boundary to that in the interior is approximately $1/(1 + 3\alpha)$. We tested α in the range $0 \leqslant \alpha \leqslant 0.75$.

3. The ADI Method

We used an alternating direction implicit method for the temperature (θ) equation which is fourth order accurate in space and second order in time. A fourth order accurate direct method was used for the stream function ψ.

The ADI scheme for the temperature is written below. A fictitious point was used along the sides of the $(\hat{x}, \hat{z})$ rectangle. Therefore the mesh is $(\hat{x}_i, \hat{z}_m)$, where $\hat{x}_i = -1 + i\,\Delta x$, $-1 \leqslant i \leqslant NX + 1$, $\hat{z}_j = -1 + j\,\Delta z$, $0 \leqslant j \leqslant NZ$, $\Delta x = 2/NX$, $\Delta Z = 2/NZ$. An equation for each of the fictitious points is obtained from the boundary conditions by using a five point approximation for $\theta_{\hat{x}} = 0$. Thus, at $\hat{x}_{-1} = -1 - \Delta x$ we have the equation

$$(-3\theta^n_{-1j} - 10\theta^n_{oj} + 18\theta^n_{1j} - 6\theta^n_{2j} + \theta^n_{3j})/(12\,\Delta x) = 0, \tag{3.1}$$

where the finite difference coefficients are chosen to yield a fourth order accurate approximation to θ_x. Here we have used θ^n_{ij} to denote the approximation at time level t_n and mesh point (x_i, z_j). A similar equation holds along the right side. In order to clarify the presentation we will write the ADI scheme for equation (2.2) in the original coordinates, rather than (2.8) in the transformed coordinates.

$$\hat{\theta}^{n+1} = \theta^n + \Delta t\, L_x \frac{(\hat{\theta}^{n+1} + \theta^n)}{2} + \Delta t\, L_z(\theta^n) - \Delta t\, \delta_x(\psi^{n+1/2}), \tag{3.2}$$

$$\theta^{n+1} = \theta^n + \Delta t\, L_x \frac{(\hat{\theta}^{n+1} + \theta^n)}{2} + \Delta t\, L_z \frac{(\theta^{n+1} + \theta^n)}{2} - \Delta t\, \delta_x(\psi^{n+1/2}). \tag{3.3}$$

At the sides the boundary condition (3.1) is used to obtain an equation for x_{-1} and x_{NX+1}. In the interior the operators are

$$L_x(\theta) = \frac{1}{R}\delta_{xx}(\theta) - \delta_z(\psi^{n+1/2})\,\delta_x(\theta),$$

$$L_z(\theta) = \frac{1}{R}\delta_{zz}(\theta) + \delta_x(\psi^{n+1/2})\,\delta_z(\theta).$$

Here $\delta_{xx}(\theta)\,|_{(x_i,z_j)} = \alpha_1\theta_{i_1,j} + \alpha_2\theta_{i_2,j} + \alpha_3\theta_{i_3,j} + \alpha_4\theta_{i_4,j} + \alpha_5\theta_{i_5,j}$ is an approximation for the second derivative $\partial^2/\partial x^2$, where the coefficients α_i are determined from polynomial interpolation thru the points $x_{i_1},\ldots, x_{i_5}$. The points are taken to be centered if possible (i.e., $x_{i-2}, x_{i-1},\ldots, x_{i+2}$) otherwise a one sided approximation is used. These approximations will yield fourth order accuracy except for the second

derivative terms $\delta_{xx}(\theta)$ and $\delta_{zz}(\theta)$ at the first mesh points in from the boundary (x_0, x_{NX}, z_1, and z_{NZ-1}). Experience with two point boundary value problems indicates that this provides global accuracy which is fourth order. The $\psi_{i,j}^{n-1/2}$ values are approximations of the stream function centered between t_n and t_{n+1}. We will discuss the computation of $\psi^{n+1/2}$ shortly. The solution of Eqs. (3.2) and (3.3) for $\hat{\theta}^{n+1}$ and θ^{n+1} require the solution of a banded linear system of equations whose total bandwidth is five, that is the matrix of the system has at most five non-zero elements in each row. A Gauss elimination routine with pivoting is used for this solution.

The equation for the stream function ψ was solved using a subroutine, SEPELI, written by Adams [16], which is available from the National Center for Atmospheric Research. This routine uses a direct method to solve a second order finite difference approximation of (2.1). To obtain fourth order accuracy, the right side ($-\theta_x$) in (2.1) is approximated by a fourth order, five point formula which is one sided near the vertical boundary of the domain. Then a deferred correction is used to obtain a fourth order accurate solution of (2.1). This involves solving an equation which is the same as (2.1) except a truncation error estimate is added to the right side as a correction term. Thus an equation like (2.1) must be solved twice, but each time a fast direct method can be used since we have a standard second order approximation of the Laplace operator. This yields the same asymptotic convergence rate (namely, $O(\Delta x^4) + O(\Delta z^4)$) as a finite difference approximation based on a five point approximation in each direction. However, the system of equations can be solved by two applications of a fast direct solver based on a three point approximation. Therefore, the method is quite efficient.

The value of ψ should be computed at $t_{n+1/2}$ in order to obtain second order accuracy in time. This requires that the derivative θ_x in (2.1) be evaluated at $t_{n+1/2}$. We tried three ways to center ψ at $t_{n+1/2}$. In the first we used linear extrapolation from θ^{n-1} and θ^n to obtain $\theta^{n+1/2}$, then compute $\psi^{n+1/2}$ from (2.1), then use a complete ADI (sweep in both the x and z directions) to compute θ^{n+1}. To start the code we set $\theta^{-1} = \theta^0$ in this case. In the second method we compute ψ^n using θ^n in (2.1), then perform the ADI sweep in x direction for $\hat{\theta}^{n+1}$, using ψ^n instead of $\psi^{n+1/2}$, then perform the ADI sweep in the z direction using $\psi^{n+1/2}$ to obtain θ^{n+1}. This requires two solutions of (2.1) and one complete ADI step for (2.2). In the third method we compute ψ^n from θ^n, use one complete ADI step to compute a first approximation to θ^{n+1} based on ψ^n instead of $\psi^{n+1/2}$, then compute $\psi^{n+1/2}$ using this value of θ^{n+1}, then repeat the computation for θ^{n+1} using $\psi^{n+1/2}$. This method requires twice as much work as the first method, however, the first two methods were sometimes unstable if the timestep was too large. Also the first required a smaller time step to obtain the same accuracy as the third method. Therefore we generally used the third method for the computation of oscillatory solutions. For steady state solutions we computed ψ^n from θ^n and then used ψ^n instead of $\psi^{n+1/2}$ in the ADI sweeps. We observed no stability problems with this method.

As an option, we included a second order version of the ADI scheme. This used a three point mesh instead of the five point stencil described above. The deferred correction can be omitted from the calculation of ψ by the SEPELI code. In this case

the calculation for ψ has second order accuracy. Note that the ADI scheme is applied to the transformed equations (2.8) and (2.9).

4. The Runge–Kutta–Fehlberg Method

The program for this method is written in the form of a subroutine to solve a fairly general class of PDE problems [6]. This class includes a system of "marching equations" in the form

$$\mathbf{u}_t = f(\mathbf{w}, \mathbf{w}_x, \mathbf{w}_z, \mathbf{w}_{xx}, \mathbf{w}_{xz}, \mathbf{w}_{zz})$$

possibly coupled with a single elliptic equation for a scalar variable

$$a_1(x)\,\psi_{xx} + a_2(x)\,\psi_x + b_1(z)\,\psi_{zz} + b_2(z)\,\psi_z + (a_3(x) + b_3(z))\psi = r(\mathbf{u}, \mathbf{u}_x, \mathbf{u}_z, \mathbf{u}_{xx}, \mathbf{u}_{xz}, \mathbf{u}_{zz}).$$

Here $\mathbf{u}$ is a vector

$$\mathbf{u}(t, x, z) = (u_1(t, x, z), \ldots, u_n(t, x, z))^T$$

and w consists of u augmented by the elliptic variable ψ,

$$\mathbf{w}(t, x, z) = (u_1(t, x, z), \ldots, u_n(t, x, t), \psi(t, x, z))^T.$$

The spatial domain is a rectangle in (x, z). The numerical approximation is based on the method of lines. A finite difference approximation is used in the (x, z) domain. This results in a system of ordinary differential equations in time t for the functions $W_{ij}(t)$ which approximate the mesh point values $w(t, x_i, z_j)$. The mesh points (x_i, z_j) need not have a uniform spacing, although all of our RKF computations were carried out with a uniform mesh spacing.

The finite difference approximation in (x, z) can be either second order accurate involving three mesh points or fourth order involving five points. The Runge–Kutta–Fehlberg version which we used was taken from a report by Shampine [17]. This is an RKF 3–4 scheme which yields both third and fourth order accurate approximations in time. The difference between these approximations is used to estimate the time discretization error and control the time step. The time step is set so that the estimated error (est) is bounded by

$$\text{est} \leqslant \varepsilon_{\text{rel}} \|\theta(x, z, t_n)\| + \varepsilon_{\text{abs}}.$$

In our computations we set $\varepsilon = \varepsilon_{\text{rel}} = \varepsilon_{\text{abs}}$ and generally used ε in the range $2.E{-}5 \leqslant \varepsilon \leqslant 1.E{-}3$. This RKF 3–4 scheme is similar to the RKF 4–5 scheme [13] except it requires less storage and computation and it is less accurate. The 3–4 scheme is probably the better choice for the method of lines solutions to initial value problems in partial differential equations. The time step tends to be limited by a stability

restriction so that higher order schemes are not useful. An Adams scheme might be more efficient for our problem because the evaluation of the stream function is quite expensive on the 30×30 mesh, and the Adams sceme tends to require fewer functional evaluations. However, the Adams scheme requires too much storage. An implicit scheme, such as the higher order backward difference formulas used in the Gear codes [13, 18] would permit a larger time step. However, they would require the solution of a system of equations involving a very large Jacobian matrix. On a 30×30 mesh with a five point difference approximation the Jacobian matrix would have order 900 with bandwidth 150 (approximately).

The ADI scheme is superior to the RKF scheme when a steady state solution is desired. For oscillatory solutions the RKF tends to be more efficient. The RKF is more efficient at higher Rayleigh numbers since its time step is limited by a stability condition which depends on the reciprocal of the Rayleigh number. The RKF code, with Rayleigh number $R = 400$, mesh resolution $N = 20$, and error tolerance $\varepsilon = 2.E{-}4$, requires about 67 % as much CPU time as an ADI code with the same R and N and time step $\Delta t = 0.1$. With $N = 30$, $\varepsilon = 2.E{-}5$, and $\Delta t = 0.05$ the RKF requires about 72 % as much CPU time. The comparison is not very accurate, since the computing time depends on ε and Δt, and it is difficult to adjust these parameters to give the same accuracy. Also, the ADI code is not programmed as carefully and requires additional work due to the coordinate transformation.

The spatial finite difference approximations used in the ADI and RKF codes are not exactly the same. There are slight differences at the boundary. The RKF code was designed primarily for hyperbolic problems. Therefore the finite difference approximation for first derivatives is one lower order near the boundary than in the interior [6]. A third order one sided approximation based on four mesh points is used along the mesh lines immediately adjacent to the upper and lower boundaries. In the interior a five point centered formula is used. Along the vertical side boundary a fictitious point is used to set up a five point formula in both the RKF and ADI codes. As shown in Figs. 2 and 3 there is very little difference between the results obtained by the two codes.

5. On the Accuracy of the Steady State Solution

In this section we attempt to estimate the accuracy of our numerical solutions for values of the Rayleigh number low enough to yield steady state solutions. This enables us to comment on the value of the coordinate transformation and also on the comparison between second and fourth order schemes. In the next section we show that the time dependent oscillatory solutions at higher Rayleigh numbers require a very accurate scheme. While there is probably little need for such accuracy in most steady state computations, we need the accuracy in order to compare methods. Our comparisons will be based on the Nusselt number since it is a scalar quantity of considerable physical interest. We prefer to compare the integral of the Nusselt

number $\bar{\mathrm{Nu}}$ in the vertical rather than the value $\mathrm{Nu}(-1)$ at the lower boundary. For the true steady state solution these numbers are the same. However, the numerical computation of $\mathrm{Nu}(-1)$ requires a difference approximation of θ_z using four values of θ above the boundary along with the boundary value. This approximation is completely one sided whereas the approximation of the differential equation uses difference formulas with one point below and three points above the center point. As we will see, the boundary values $\mathrm{Nu}(-1)$ and $\mathrm{Nu}(0)$ are not as accurate as the interior values. We are indebted to one of the reviewers of this paper for observing that $\theta_{zz} = 0$ along the bottom and top boundaries in the case that $\theta = 0$ there. It is easy to show that $\partial^4\theta/\partial z^4 = 0$ as well. The reviewer suggests the use of skew symmetry for the boundary condition in θ and in the θ_z computation for the Nusselt number. This would probably have yielded better accuracy than our method. Our code was designed for a variable temperature along the boundary for which the skew symmetry condition is not suitable. However, we could have used a special boundary calculation for the $\theta = 0$ case.

For all of the steady state cases at $R = 200$ we used the initial function

$$\theta = -\sin \pi z \cos \pi x, \qquad -1 \leqslant z \leqslant 0. \tag{5.1}$$

These runs were made with the ADI code unless a statement is made to the contrary. We turn next to a discussion of the results. In all of these steady state cases we chose Δt to give fast convergence, usually $\Delta t = 2.0$.

5.1. *A Richardson Extrapolation for the Nusselt Number*

We used an equally spaced mesh in (x, z) with the mesh spacing given by $h = 1/N$. The Richardson extrapolation is based on an assumed expansion of the Nusselt number, namely,

$$\bar{\mathrm{Nu}}(h) = N_0 + N_1 h^p + O(h^{p+1})$$

Here p is the order of scheme, $p = 2$ or $p = 4$ for our codes. Computation of $\bar{\mathrm{Nu}}(h)$ at two values of the mesh spacing (h_1, h_2) enables elimination of the $N_1 h^p$ term to give the extrapolated value N_0 provided the $O(h^{p+1})$ term is ignored. These extrapolated values based on the pairs (1/20, 1/30), (1/30, 1/40), and (1/40, 1/50) are shown in Table I. For these runs the coordinate transform parameter α has the value, $\alpha = 0.25$. The agreement between the extrapolated values appears to be very good. We will assume the value for the pair (1/40, 1/50) is the true value. In subsequent discussion the error will be computed from this last extrapolated value $\bar{\mathrm{Nu}} = 3.809796$. Note that we will compare the integral Nusselt number $\bar{\mathrm{Nu}}$ and not the boundary number $\mathrm{Nu}(-1)$. The corresponding value of Nusselt number found from Caltagirone's second order method, for $N = 48$, is $\bar{\mathrm{Nu}} = 3.813$. Relative to the results in Table I only three place accuracy is achieved, even with the high level of resolution, $N = 48$. A Galerkin calculation by Schubert and Straus [12] using 30 modes gave a more accurate value, $\bar{\mathrm{Nu}} = 3.808$. A symmetry condition was invoked in order to set the

TABLE I

Richardson Extrapolation for $\bar{\mathrm{Nu}}$, Based on the Fourth Order Scheme with the Coordinate Transform Parameter $\alpha = 0.25$

N	$\bar{\mathrm{Nu}}$	Extrapolated $\bar{\mathrm{Nu}}$
20	3.812011	—
30	3.810179	3.809728
40	3.809908	3.809783
50	3.809842	3.809796

Note. Here $\Delta\hat{x} = \Delta\hat{z} = 2/N$.

amplitude of a variety of non-symmetric modes equal to zero a priori. It is not obvious how this assumption affects the Nusselt number value obtained.

5.2. *The Influence of the Coordinate Transform*

We believed that a coordinate transform which concentrated points in the boundary layer would improve the accuracy. However, this was not generally the case. The coordinate transformation is described in Section 3. The ratio of the mesh spacing at the boundary to that in the interior is given by $1/(1+3\alpha)$. For $\alpha = 0.75$ this yields 0.31 for the ratio. Here α is the parameter which defines the coordinate transform. In Table II we give the variation of the integral Nusselt number ($\bar{\mathrm{Nu}}$) with α. Here the spatial resolution was $h = 1/N = 1/20$. The Nusselt number $\mathrm{Nu}(z)$ was computed on each horizontal line of the mesh. The maximum and minimum of these values taken over the interior (i.e., excluding the upper and lower boundary) is also shown along with the boundary value. These Nusselt numbers were always symmetric about the center of the mesh, therefore the two boundary values are equal. The error is determined by using the extrapolated value given in Section 5.1 above. The value $\alpha = 0.5$ gives a minimum spread in the interior values of $\mathrm{Nu}(z)$ and gives almost as good an error as $\alpha = 0.75$. Except for the boundary values the larger values of α give somewhat better results. The difficulty at the boundary is a surprise, since the mesh points are closer at the boundary. This behavior may depend on the resolution N. We made the comparison for different values of α only at $N = 20$, and $R = 200$ where the boundary layers are not as well developed.

In Table III we show the error in $\bar{\mathrm{Nu}}$ and also the spread of the interior values of $\mathrm{Nu}(z)$ for $\alpha = 0.0$. Note that the difference in the extrapolated values of $\bar{\mathrm{Nu}}$ between the pair (1/20, 1/30) and (1/40, 1/50) is about $50.E{-}5$ whereas it is $7.E{-}5$ for $\alpha = 0.25$ in Table I. Also we have a sharp minimum in the error at $N = 40$. This is probably due to some sort of "error cancellation" in the computation of $\bar{\mathrm{Nu}}$. Such cancellation would tend to create inaccuracy in the asymptotic expansion used for the Richardson extrapolation. These results do not show any advantage in using more

TABLE II

Accuracy of Nu as Function of Coordinate Transform Parameter α

α	$\bar{\text{Nu}}$	Nu(min)	Nu(max)	Nu boundary	Nu(max) − Nu(min)	Error in $\bar{\text{Nu}}$
0.	3.80688	3.8031	3.8142	3.8222	1.1 *E*–2	2.9 *E*–3
0.25	3.81201	3.8114	3.8179	3.7566	6.5 *E*–3	2.2 *E*–3
0.5	3.81144	3.8104	3.8150	3.7770	4.6 *E*–3	1.6 *E*–3
0.75	3.81092	3.8077	3.8130	3.7908	5.3 *E*–3	1.1 *E*–3

Note. Here $R = 200$, $N = 20$, ADI scheme.

TABLE III

Error in the Nusselt Number at $\alpha = 0.0$, $R = 200$

N	$\bar{\text{Nu}}$	Extrapolated $\bar{\text{Nu}}$	Nu(max) − Nu(min)	Error in $\bar{\text{Nu}}$
20	3.806883	—	1.1 *E*–2	2.9 *E*–3
30	3.809637	3.810315	2.3 *E*–3	1.6 *E*–4
40	3.809797	3.809871	9.9 *E*–4	1.0 *E*–6
50	3.809807	3.809814	4.5 *E*–4	1.1 *E*–5

TABLE IV

Error in $\bar{\text{Nu}}$ for Second and Fourth Order ADI with $\alpha = 0.25$

	Error	
N	Second order	Fourth order
20	3.8 *E*–2	2.2 *E*–3
30	1.5 *E*–2	3.8 *E*–4
40	8.4 *E*–3	1.1 *E*–4
50	5.2 *E*–3	4.6 *E*–5

TABLE V

Computing Time in Seconds per Time Step on the CDC 6400

Resolution, scheme	Total time	θ Equation time	ψ Equation time	Other time
$N = 20$ second order	1.59	0.75	0.65	0.19
$N = 40$ second order	6.48	2.93	2.90	0.65
$N = 20$ fourth order	2.74	1.00	1.52	0.22
$N = 40$ fourth order	9.73	3.63	5.43	0.67

Note. One evaluation of ψ per time step, ADI scheme.

points within the boundary layer. In fact, for $N = 30$ the values of $\bar{\text{Nu}}$ obtained with $\alpha = 0$ are considerably superior to those with $\alpha = 0.25$. Due to the cost, we did not run more experiments with variable α at a higher mesh resolution, say $N = 30$.

5.3. *Second vs Fourth Order Accuracy*

In Table IV a comparison of the second and fourth order ADI schemes is given for the case $R = 200$. The error for the former when $N = 50$ is of the order of magnitude of the difference between the present result and that given by Caltagirone [1]. In Table V a sample of computing time on a CDC 6400 is given. The "other time" category includes the computation of the Nusselt number, which is done on each time step. A further indication of accuracy is given in Table VI where the variation in the Nusselt number $\text{Nu}(z)$ is given. Again the spread $(\text{Nu(max)} - \text{Nu(min)})$ in the Nusselt numbers refers only to the interior values, the boundary values are excluded. The Nusselt number values obtained from the second order scheme for $N = 50$ are close to that given by Caltagirone. To obtain a given accuracy, even at relatively low accuracy, the fourth order scheme appears to be less expensive.

Horne has also used a fourth order scheme for these equations [19]. However, he felt it was necessary to have high accuracy only in the θ equation. He used second order accuracy for the stream function ψ. His comparison was more qualitative, and he was mainly interested in time dependent solutions. In Table VII we show a comparison of second and fourth order methods for the stream functions as applied to be steady state problem at $R = 200$. The fourth order θ and second order ψ scheme does yield a considerable improvement over the purely second order case. However, the purely fourth order scheme is still better and its use would appear to be justified from a cost effectiveness point of view.

TABLE VI

Comparison of Nusselt Number Variation for a Second and Fourth Order Scheme

N	Nu(min)	Nu(max)	Nu(max) − Nu(min)	Nu (boundary)
		Second order scheme		
20	3.82906	3.88339	5.4 E–2	3.83743
30	3.81738	3.83867	2.1 E–2	3.82776
40	3.81377	3.82525	1.1 E–2	3.82137
50	3.81223	3.81962	7.4 E–3	3.81762
		Fourth order scheme		
20	3.81138	3.81782	6.4 E–3	3.75654
30	3.80991	3.81146	1.6E–3	3.79760
40	3.80979	3.81029	5.0 E–4	3.80608
50	3.80978	3.80999	2.1 E–4	3.80834

Note. ADI with $\alpha = 0.25$.

TABLE VII

Dependence of Error on the ψ Scheme

	$N = 20$		$N = 30$	
	Error in $\bar{\text{Nu}}$	CPU time per step	Error in $\bar{\text{Nu}}$	CPU time per step
2nd order θ 2nd order ψ	3.8 E–2	1.59	1.5 E–2	3.55
4th order θ 2nd order ψ	9.5 E–3	1.84	3.5 E–3	4.00
4th order θ 4th order ψ	2.2 E–3	2.74	3.8 E–4	5.25

Note. One solution of ψ equation per time step. $\alpha = 0.25$. CPU time in seconds on a CDC 6400.

6. The Nature of the Oscillatory Solution

When the Rayleigh number is increased, the steady convection solution becomes unstable. An oscillation in time is observed. This is most easily seen by plotting the Nusselt number as a function of time. We will again plot the integral Nusselt number because we feel it can be computed more accurately than the boundary Nusselt number. However, we will also refer to the latter, since it is of greater relevance. This instability or breakdown has been studied by several people. Horne and O'Sullivan

[8, 9] found the transition to oscillation at $R = 280$, Schubert and Straus [12] at $300 < R < 320$, and Caltagirone [1] at $R = 384$. Horne and O'Sullivan's computation found this to be a harmonic oscillation with a fairly well defined period at higher R ($R \simeq 750$) provided only half the bottom surface was heated. If the entire bottom surface is held at a uniform temperature then the oscillation in the Nusselt number was irregular with no well defined period or amplitude. Horne and O'Sullivan and also Schubert and Straus have found that a steady multicellular solution can be obtained if the proper initial conditions are used. Our results are similar. In addition we find a nearly steady single cell solution and oscillatory solutions of apparently different structure depending on the initial conditions.

6.1. *Accuracy in the Oscillatory Case*

The oscillatory case seems to require much greater resolution than the steady case discussed above. In the next section we show that the oscillation has a finer scale than the steady solution. This would explain the need for higher resolution. The cases which we describe in this section all use the steady state solution at $R = 300$ as the initial condition with Rayleigh number $R = 400$ used throughout the computation. The steady state solution at $R = 300$ is obtained from the ADI scheme, then saved on a file and used to start both the ADI and RKF schemes at the higher Rayleigh number ($R = 400$). In Table VIII the amplitude of the oscillation in the Nusselt number is given, both for the integrated Nusselt number $\bar{\text{Nu}}$ and the boundary value

TABLE VIII

Minimum and Maximum Values of the Nusselt Number—Dependence on Method and Resolution

Method and resolution	Integral Nusselt, $\bar{\text{Nu}}$		Boundary Nusselt Nu(−1)	
	Min	Max	Min	Max
RKF, $N = 20$	4.81	5.24	5.18	5.31
ADI, $N = 20$ $\alpha = 0.25, \Delta t = 0.1$	4.77	5.48	4.92	5.17
RKF, $N = 30$	4.91	5.15	4.99	5.07
ADI, $N = 30$ $\alpha = 0.25, \Delta t = 0.05$	4.90	5.19	4.97	5.06
ADI, $N = 30$ $\alpha = 0.0, \Delta t = 0.05$	4.90	5.16	5.00	5.08
RKF, $N = 20$ Second order	4.83	5.64	5.49	5.83

Note. $R = 400$.

Nu(−1). These are minimum and maximum values over the interval $90 \leqslant t \leqslant 100$ with the calculation started at $t = 0$. The Nusselt number is printed at each time step of the Runge–Kutta code (RKF) and at intervals of $\Delta t = 0.2$ for the ADI code. The time step used by RKF varied around 0.4. The error tolerance for RKF was $\varepsilon =$ 2.*E*–5 for both relative and absolute parts of the error. Judging from runs with mesh resolution $N = 20$, this value of ε is small enough so that time discretization error is not significant. Schubert and Straus report a Nusselt number range of 5.09–5.45 at $R = 400$ which is somewhat larger than our range of 4.99–5.07. It is difficult to judge the accuracy of our results. We need a run at $N = 40$ to verify convergence, but the cost is too high to permit us to make such a run given the computer available.

The ADI scheme was run with a fixed time step. Experiments were run at $N = 20$ which indicate that the time step, $\Delta t = 0.1$, is small enough so that temporal error is not significant.

6.2. *The Nature of the Oscillation*

The variation of the integral Nusselt number $\bar{\text{Nu}}$ with time is shown in Fig. 1. This computation was performed by the RKF scheme with $N = 30$ and $R = 400$. The steady state solution at $R = 300$ was used as the initial condition at $t = 0$. The time runs along the x-axis from $0 \leqslant t \leqslant 100$. The period of the oscillation is quite well defined although the amplitude varies somewhat. This period is about 4.7 time units and seems to be largely independent of the finite difference resolution. The corresponding value of Schubert and Straus is 4.8. The amplitude, however is quite dependent on the resolution as Table VIII indicates. Figure 2 shows the same Nusselt

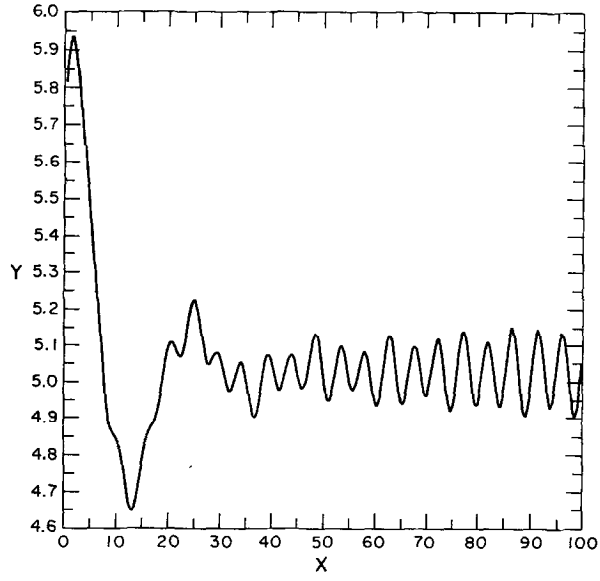

FIG. 1. The Nusselt number $\bar{\text{Nu}}(t)$ by RKF scheme, $N = 30$, $R = 400$.

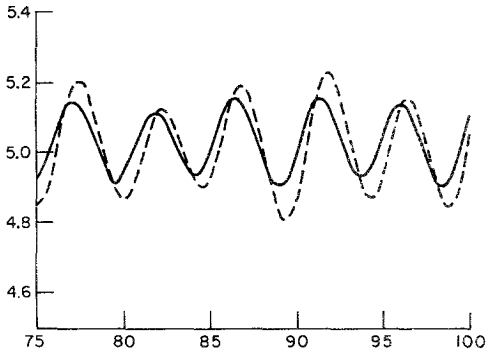

FIG. 2. $\bar{\mathrm{Nu}}(t)$ obtained by RKF scheme, $R = 400$. The --- curve has $N = 20$, the —— curve has $N = 30$.

number plotted for $75 \leqslant t \leqslant 100$. Two curves are drawn, one for the resolution $N = 20$, the second for $N = 30$. Both curves were made by the RKF scheme at $R = 400$. Figure 3 shows the same problem solved by the ADI scheme. One curve is obtained when the coordinate parameter has the value $\alpha = 0.25$. The curve for $\alpha = 0.0$ is almost identical with the RKF case. The ADI and RKF schemes use almost the same spatial difference approximation. Therefore if the temporal error is small we would expect the two schemes to yield the same result.

In Fig. 4 a contour plot of the time-averaged temperature is shown. Note that this is a deviation from the linear conduction temperature and not the total temperature. This value is computed by summing the temperature at each grid point over all the time steps for $95 \leqslant t \leqslant 100$ then dividing by the number of time steps. A similar plot of the stream function is given in Fig. 5. The maximum values of θ and ψ at $t = 100$, obtained by the ADI scheme with $N = 30$ and $\alpha = 0.0$ are $\theta_{\max} = 0.560$ and $\psi_{\max} = 0.0330$.

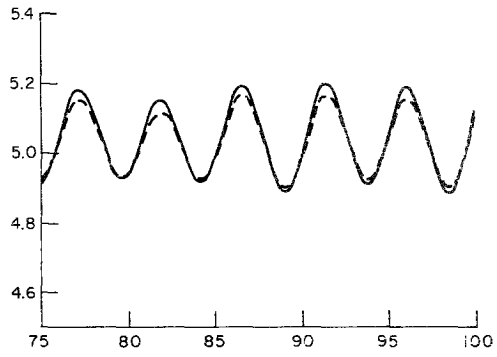

FIG. 3. $\bar{\mathrm{Nu}}(t)$ obtained by ADI scheme, $R = 400$, $N = 30$. The --- curve has $\alpha = 0.0$, the —— has $\alpha = 0.25$.

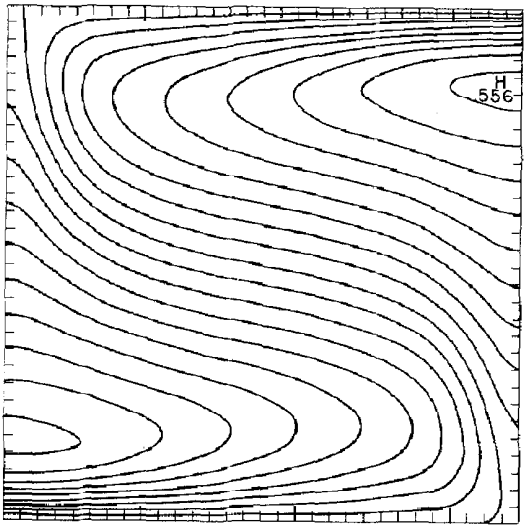

FIG. 4. Temperature $\theta(x, z)$ obtained by RKF, $R = 400$, $N = 30$. Averaged for $95 \leqslant t \leqslant 100$.

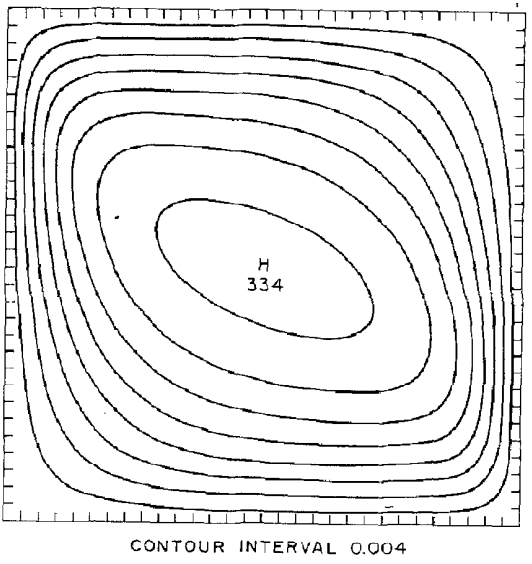

FIG. 5. Stream function $\psi(x, z)$ obtained by RKF, $R = 400$, $N = 30$. Averaged for $95 \leqslant t \leqslant 100$.

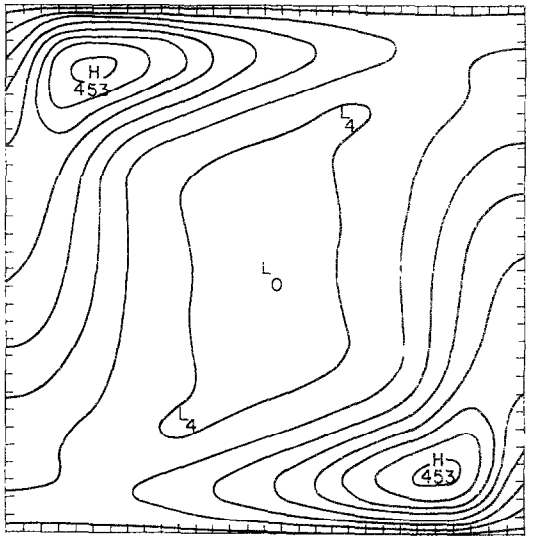

FIG. 6. Oscillation amplitude in $\theta(x, z)$ for $95 \leqslant t \leqslant 100$. Obtained by RKF, $R = 400$, $N = 30$.

In Fig. 6 a contour plot of the amplitude of the oscillation in θ is shown. This is the difference of the maximum and minimum values at each mesh point in the interval $95 \leqslant t \leqslant 100$. A similar plot for the stream function is given in Fig. 7. The amplitude of the oscillation in θ is 0.045 and for ψ it is $2.2E{-}3$. The amplitude relative to the values of θ_{max} and ψ_{max} are 0.081 and 0.065. The relative amplitude of

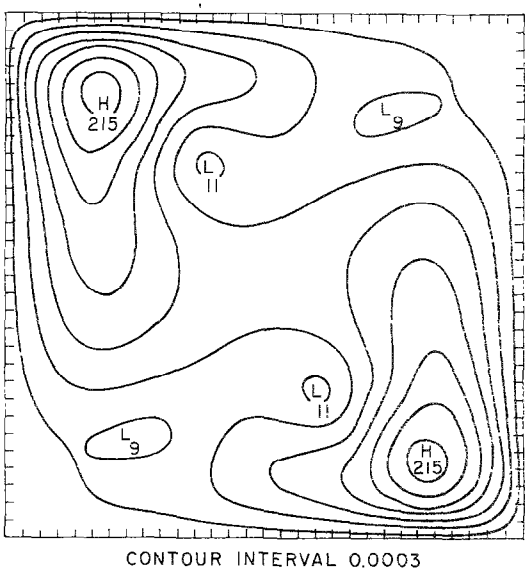

FIG. 7. Oscillation amplitude in $\psi(x, z)$ for $95 \leqslant t \leqslant 100$. Obtained by RKF, $R = 400$, $N = 30$.

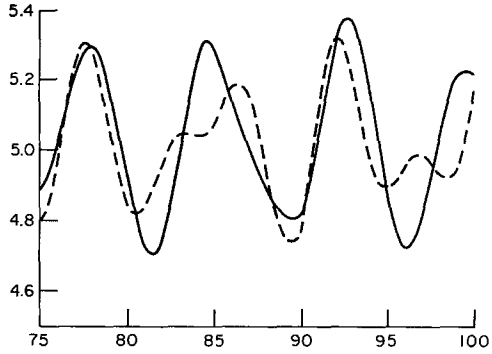

FIG. 8. $\bar{\mathrm{Nu}}(t)$ obtained by RKF scheme at $R = 400$ and $N = 20$. —— started from steady solution at $R = 200$, --- at $R = 225$.

the oscillation in the integral Nusselt number is $0.24/5.02 = 0.048$. Note that the oscillation is concentrated in the corners. The fluid flows upward on the right side of the domain. The oscillation has a more rapid spatial variation than the average values. If the instantaneous values of θ and ψ are plotted for several values of t, the plots are almost the same as the plots of the average values. There is a small but noticeable deviation in some contour lines due to the oscillation.

One may infer from Figs. 6 and 7 that the relatively cool liquid moves downward along the left boundary then turns the corner with only minor variations in time at a given location. Then as the liquid moves to the right along the lower hot boundary,

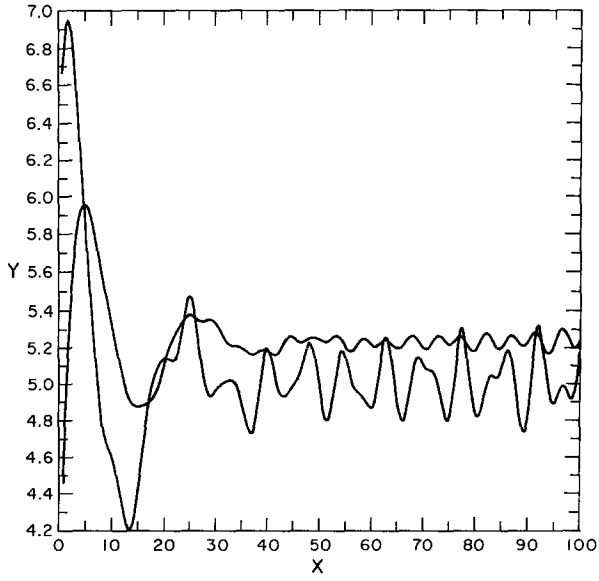

FIG. 9. Nusselt numbers $\bar{\mathrm{Nu}}$ and $\mathrm{Nu}(-1)$ (upper curve) as a function of t $(0 \leqslant t \leqslant 100)$ at $R = 400$, $N = 20$, from RKF started from steady solution at $R = 225$.

absorbing heat, an instability develops which is manifested as relatively large amplitude oscillations in the lower right-hand corner. Since the porous media momentum equation contains no inertia term the instability is not connected with nonlinear inertial effects. Rather, it appears that a thermal instability develops in the outer portion of the heated layer adjacent to the hot boundary. Since the larger amplitude variations are several mesh spacings from the boundary the process does not appear to involve a separation process. It is noted that the area of the stream function variation to half the maximum value is confined to a narrow region above the location of maximum variation while the analagous thermal disturbance area is larger and extends upwards and to the right. Hence, some of the thermal variations in time apppear to be occurring where the stream function is relatively steady. Eventually conduction smooths out the variation.

The nature of the oscillation was strongly influenced by the initial condition in θ and ψ used to start the calculation. If the analytic functions of Eq. (5.1) are used to start a calculation at $R = 400$ then a steady multicellular solution is obtained (see the next section). If the calculation is started at $R = 400$ using the steady solution obtained at $R = 200$ or $R = 225$ an oscillation in $\bar{\mathrm{Nu}}(t)$ quite different from that shown in Figs. 1 thru 3 is obtained. The results of using $R = 200$ and $R = 225$ are shown in Fig. 8 which can be compared with Fig. 2. The case started with the steady solution at $R = 225$ is also shown in Fig. 9 for the interval $0 \leqslant t \leqslant 100$. The upper curve is the boundary Nusselt number $\mathrm{Nu}(-1)$. It would appear from this graph that the motion is possibly periodic, but certainly not harmonic.

We made an attempt to determine minimum Rayleigh number at which an oscillatory solution can be found. The nature of the oscillation seems to be highly dependent on the initial conditions used to start the integration. Therefore, any experimental attempt to find the minimum should probably use several different initial conditions. We used only two initial conditions. These were the steady state solution obtained at $R = 300$ using the ADI scheme and a perturbation of this solution obtained by adding the following field to the initial temperature

$$\begin{array}{ll} a(1 + \cos 4\pi x)(1 + \cos(4\pi(z + 0.25))), & 0.25 \leqslant x \leqslant 0.75 \\ & -1 \leqslant z \leqslant -0.5 \\ 0 & \text{otherwise.} \end{array} \tag{6.1}$$

The value of the amplitude parameter was $a = 0.05$ which gives about a 10 % perturbation in θ. Using the steady solution at $R = 300$ to start a calculation at $R = 400$ does produce an oscillation as we have seen. However, this steady solution with the 10 % perturbation of θ did not yield an oscillatory solution when used to start a calculation at $R = 350$. This suggests the oscillation starts somewhere between $R = 350$ and $R = 400$. Straus and Schubert found the onset of oscillation to occur at $R = 300$ to $R = 320$. Their calculation used a Galerkin method which they checked for accuracy by varying the resolution. Their initial condition differed from ours, which probably accounts for the different result.

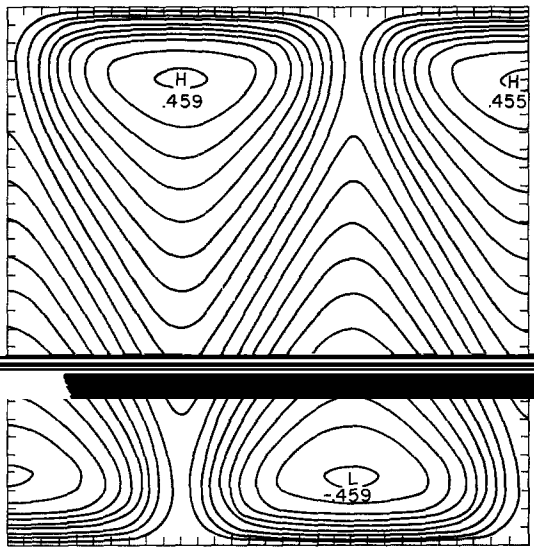

FIG. 10. Temperature $\theta(x, z)$ obtained by ADI, $R = 400$, $\alpha = 0.25$, $N = 30$, started at $R = 400$ using (5.1).

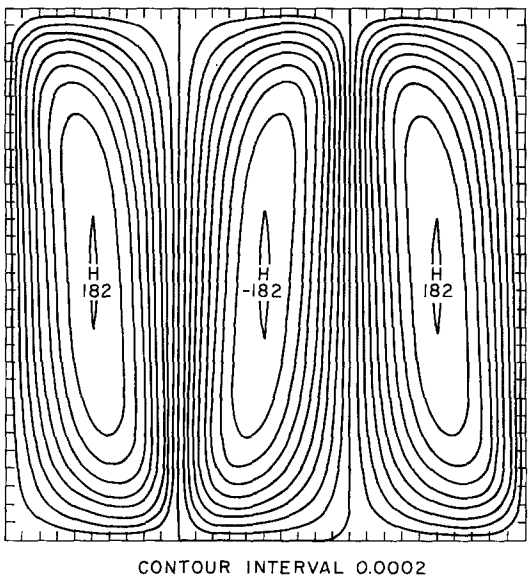

FIG. 11. Stream function $\psi(x, z)$ obtained by ADI, $R = 400$, $\alpha = 0.25$, $N = 30$, started at $R = 400$ using (5.1).

6.3. *Steady State Solutions*

If the analytic formula of Eq. (5.1) is used to start a calculation at $R = 400$, then a steady state solution with a Nusselt number near 6.1 is obtained. This solution has the multicellular form shown in Figs. 10 and 11. The Nusselt number obtained for resolution $N = 30$, coordinate transform $\alpha = 0$ is $\bar{\mathrm{Nu}} = 6.11$, for $N = 30$, $\alpha = 0.25$, $\bar{\mathrm{Nu}} = 6.17$, for $N = 20$, $\alpha = 0$, $\bar{\mathrm{Nu}} = 5.86$, and for $N = 20$, $\alpha = 0.25$, $\bar{\mathrm{Nu}} = 6.12$. Schubert and Straus report Nusselt number values of 5.897, 6.045 and 6.108 for increasingly refined resolution defined in terms of mode numbers 10, 12 and 14.

A nearly steady solution can also be obtained at $R = 400$ provided the Rayleigh number is increased gradually from $R = 300$ to $R = 400$. We started with the steady solution at $R = 300$ with $N = 30$. Then we increased R linearly with time, starting at $t = 0$, so that $R = 400$ at $t = 50$. Then we ran with R at the constant value $R = 400$ for $50 \leqslant t \leqslant 100$. The solution reached a nearly steady state with the Nusselt number $\bar{\mathrm{Nu}} = 5.02$ at $t = 100$. The oscillation amplitude in the Nusselt number in the range $65 \leqslant t \leqslant 100$ was approximately 5.024 to 5.031. The period of the oscillation was quite uniform with a value 4.8. The oscillation amplitude varied slightly, the minimum for $65 \leqslant t \leqslant 100$ was in the range 5.0235 to 5.0240. The period of this very weak oscillation is the same as that for the case shown in Fig. 1. Apparently the oscillation is harmonic with a definite period provided it is not too strong. The amplitude apparently depends on the initial conditions. We prefer to include this case with the steady solutions since the amplitude is so small compared to the probable error in the integration.

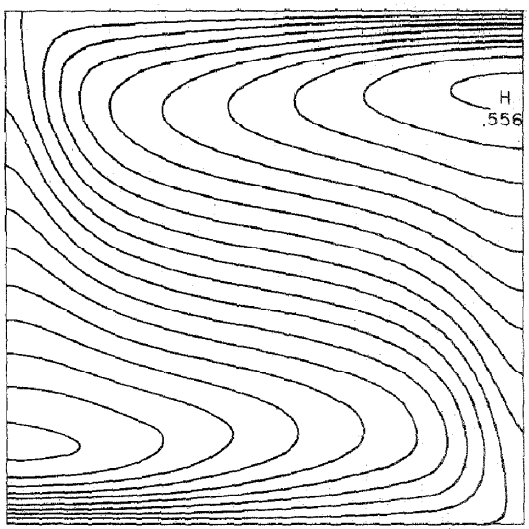

FIG. 12. Temperature $\theta(x, z)$ obtained by RKF, $R = 400$, $N = 30$, using $R(t) = 300 + 2t$ for $0 \leqslant t \leqslant 50$, $R(t) = 400$ for $50 \leqslant t \leqslant 100$.

7. Conclusions

In so far as the question of accuracy is concerned it is clear that fourth order methods are essential for obtaining long-time oscillatory results. Even with high levels of spatial resolution second order methods give less definitive solutions.

Our results appear to indicate that initial conditions and the time history of the key parameter R play a significant role in determining the long-time flow configuration. Each of the rather different modes found at $R = 400$, appear to be stable. It is reasonable to assume that strong disturbances are required to cause a transition from one to another.

For the problems described in this paper the Galerkin method is probably more efficient than the finite difference method which we used. However, we intend to extend our model to allow the material properties to vary with temperature. In this case the elliptic operator for ψ has variable coefficients which creates a problem for the Galerkin or pseudo-spectral approach [14].

References

1. J. P. Caltagirone, *J. Fluid Mech.* **72** (1975), 269–287.
2. P. Cheng, *in* "Advances in Heat Transfer," Vol. 14 (T. F. Irvine and J. P. Hartnett, Eds.), pp. 1–104, Academic Press, New York/London, 1978.
3. M. A. Combarnous and S. A. Bories, *in* "Advances in Hydroscience," Vol. 10 (Chow Vente, Ed.), pp. 231–307, Academic Press, London/New York, 1975.
4. E. Fehlberg, "Low Order Classical Runge–Kutta Formulas with Stepsize Control and their Application to Some Heat Transfer Problems," NASA T.R. 315 (1969).
5. J. Gary, *J. Comput. Phys.* **26**(3) (1978), 339–351.
6. J. Gary, RKFPDE, subroutine library, National Center for Atmospheric Research, Boulder, CO.
7. G. Hall and J. M. Watt, Eds., "Modern Numerical Methods for Ordinary Differential Equations," Oxford Univ. Press (Clarendon), London/New York, 1976.
8. R. N. Horne and M. J. O'Sullivan, *J. Fluid Mech.* **66** (1974), 339–352.
9. R. N. Horne and M. J. O'Sullivan, *Phys. Fluids* **21**(8) (1978), 1260–1264.
10. G. I. Marchuk, "Methods of Numerical Mathematics," Springer-Verlag, Berlin/New York, 1975.
11. A. R. Mitchell, "Computational Methods in Partial Differential Equations," Wiley, New York, 1969.
12. G. Schubert and J. Straus, *J. Fluid Mech.* **94** (1979), 25–38.
13. L. Shampine, H. Watts, and S. Davenport, *SIAM Rev.* **18** (1976), 376–411.
14. J. Straus and G. Schubert, *J. Fluid Mech.* **87**(2) (1978), 385–394.
14a. D. Gottlieb and S. Orszag, "Numerical Analysis of Spectral Methods," SIAM, Philadelphia, PA., 19103, 1977.
15. A. Zebib and D. Kassoy, *Phys. Fluids* **21** (1978), 1–3.
16. J. Adams, SEPELI, subroutine library, National Center for Atmospheric Research, Boulder, CO.
17. L. Shampine, unpublished manuscript.
18. L. Shampine and W. Gear, *SIAM Rev.* **21**(1) (1979), 1–18.
19. R. Horne, "Transient Effects in Geothermal Convective Systems," Ph.D. thesis, University of Auckland, New Zealand, 1975.
20. M. A. Combarnous, *in* "Proceedings, 6th International Heat Transfer Conference," Vol. 6, pp. 45–59, 1978.
21. R. N. Horne and M. J. O'Sullivan, ASME Preprint, 77-HT-56, 1977.